Multi-View 3D Reconstruction for Construction Site Monitoring

Guangan Chen[a], Michiel Vlaminck[b], Wilfried Philips and Hiep Luong[c]
Image Processing and Interpretation (IPI), imec Research Group at Ghent University,
Department of Telecommunications and Information Processing (TELIN), Ghent University, Belgium

Keywords: Construction Progress Monitoring, Structure-from-Motion, Multi-View Stereo, Point Cloud Registration.

Abstract: Monitoring construction sites is pivotal in effective construction management. Building Information Modeling (BIM) is vital for creating detailed building models and comparing actual construction with planned designs. For this comparison, a 3D model of the building is often generated using images captured by handheld cameras or Unmanned Aerial Vehicles. However, this approach does not provide real-time spatial monitoring of on-site activities within the BIM model. To address this challenge, our study utilizes fixed cameras placed at predetermined locations within an actual construction site. We captured images from these fixed viewpoints and used classical multi-view stereo techniques to create a 3D point cloud representing the as-built building. This point cloud is then aligned with the as-planned BIM model through point cloud registration. In addition, we proposed an algorithm to convert SfM reprojection error into a value with metric units, resulting in a mean SfM reprojection error of 4.17 cm. We also created voxel volumes to track and visualize construction activities within BIM coordinate system, enhancing real-time site monitoring and improving construction management.

1 INTRODUCTION

Construction site monitoring is a cornerstone in the architecture, engineering, and construction industry, acting as a vital mechanism to ensure that the progression of projects is in alignment with predetermined schedules and designs. Accurate progress reporting can enable stakeholders to make effective decisions according to the as-built states and may prevent the project from cost overruns and construction delays (Sami Ur Rehman et al., 2022; Kim et al., 2009; Oh et al., 2004).

Traditional construction progress monitoring (CPM) methods rely on manual and labor-intensive processes for gathering information, documenting, and periodically reporting the status of a construction project, which are tedious, slow, and susceptible to errors, often yielding redundant information (Sami Ur Rehman et al., 2022).

Computer Vision (CV), an advanced technology that processes visual inputs like photos or videos has emerged as a leading advanced solution in the field of automated CPM. The typical procedure of CV-based CPM includes data acquisition, information retrieval, progress estimation, and output visualization (Sami Ur Rehman et al., 2022).

Data acquisition involves applying image sensors from various devices like handheld and fixed on mounts cameras, or Unmanned Aerial Vehicles (UAVs), to collect visual as-built data. UAVs are highly effective in covering large, remote areas but face flight restrictions (Kim et al., 2019; Sami Ur Rehman et al., 2022). Handheld cameras are portable and detail-oriented but are user-dependent and prone to errors (Sami Ur Rehman et al., 2022; Golparvar-Fard et al., 2009). Fixed cameras, on the other hand, positioned at consistent elevations, offer automated and reliable data collection in varied weather, which is ideal for real-time and long-term construction monitoring (Sami Ur Rehman et al., 2022).

The information retrieval process aims to extract valuable insights from visual data, typically forming an as-built 3D model for comparison with the as-planned model to assess progress. Multi-view stereo (Furukawa et al., 2015) serves as a cost-effective technique to transform 2D images into 3D models, although with less precision compared to Lidar (Sepasgozar et al., 2014), and demands considerable processing time for larger vision datasets (Sami Ur Rehman et al., 2022).

[a] https://orcid.org/0000-0002-2238-483X
[b] https://orcid.org/0000-0003-3986-823X
[c] https://orcid.org/0000-0002-6246-5538

Chen, G., Vlaminck, M., Philips, W. and Luong, H.
Multi-View 3D Reconstruction for Construction Site Monitoring.
DOI: 10.5220/0012308300003660

In *Proceedings of the 19th International Joint Conference on Computer Vision, Imaging and Computer Graphics Theory and Applications (VISIGRAPP 2024) - Volume 4: VISAPP*, pages 469-476
ISBN: 978-989-758-679-8; ISSN: 2184-4321

Progress estimation in CV-based CPM aims to compare the as-built point cloud to as-planned Building Information Models (BIMs) (Azhar, 2011; Sami Ur Rehman et al., 2022). This comparison can be conducted by BIM registration, i.e., point cloud registration, which includes coarse registration and fine registration (Besl and McKay, 1992).

Output visualization displays insights from information retrieval or progress estimation. Activities are typically annotated on 2D images using bounding boxes (Karsch et al., 2014). Advanced methods leverage Augmented Reality (AR) and Virtual Reality (VR) to merge the BIM model with the as-built scene for an immersive construction progress view (Ahmed, 2019).

Despite the potential of CV-based CPM to improve construction monitoring by automating processes and reducing reliance on labor-intensive methods, the generation of an as-built 3D point cloud requires the collection of a large dataset from construction sites, which is a labor-intensive task (Xue et al., 2021; Sami Ur Rehman et al., 2022).

As the use of surveillance cameras for monitoring construction sites continues to spread, the utilization of the vast amount of images and videos captured daily for as-built information extraction gains more attention. In our study, we utilized images obtained from surveillance cameras to generate as-built point clouds, followed by a comparison with the BIM model. Using the homography derived from this comparison, we tracked on-site activities by forming voxel volumes of workers and integrated these volumes into the BIM model for visualization.

Our main contributions can be summarized as follows:

i. We collected a dataset consisting of images from eight different viewpoints of a real-world construction site, capturing images both day and night throughout the construction period.

ii. We propose an integrated pipeline to generate 3D point clouds from construction sites using imagery from fixed cameras and to match them with existing BIM models.

iii. We validated our pipeline by performing an experiment on a fixed-camera dataset of a real construction site for which a BIM model is available.

2 RELATED WORK

2.1 CV-Based CPM

Comparing an as-built building to a BIM model for monitoring construction progress has been studied for years (Tuttas et al., 2017; Mahami et al., 2019; Khalid Masood et al., 2020). Tuttas *et al.* (Tuttas et al., 2017) proposed a procedure for continuous construction progress monitoring. The procedure begins with the placement of markers on the initial construction site. These markers serve as feature points in the structure-from-motion (Furukawa et al., 2015) process. This setup allows the collected images on the required dates to be accurately registered in the SfM step, resulting in the generation of an accurate as-built point cloud, which is then compared to a BIM model. Likewise, Mahami *et al.*(Mahami et al., 2019) employed coded targets affixed to walls as distinctive features to enhance the precision of estimated camera poses. The authors used handheld cameras to collect images of a building, followed by creating an as-built point cloud of the building using multi-view stereo (Furukawa et al., 2015) and comparing the generated point cloud with BIM model. Masood *et al.* (Khalid Masood et al., 2020) deployed two crane camera developed by Pix4D [1] to capture images of the entire construction process, and the as-built point cloud was generated by the Pix4D system. The authors aligned the point cloud with the BIM model using the georeferencing of the point cloud.

2.2 Image-Based 3D Reconstruction

Image-based 3D reconstruction has been an active research area for several decades, intending to reconstruct 3D structures from multiple 2D images captured from different viewpoints (Furukawa et al., 2015; Hartley and Zisserman, 2003). A typical pipeline for 3D Reconstruction includes structure-from-motion (SfM) and multi-view stereo (MVS), where SfM yields the camera poses and a sparse point cloud and MVS creates dense point clouds using the estimated camera poses obtained by SfM (Furukawa et al., 2015; Hartley and Zisserman, 2003).

In addition, frameworks for SfM and MVS are proposed, such as COLMAP (Schönberger and Frahm, 2016), OpenSfM [2], and OpenMVS [3]. However, creating a 3D point cloud for an ultra-large-scale scene with sparse viewpoints remains challenging (Zhang et al., 2021).

[1] https://www.pix4d.com/

[2] https://github.com/mapillary/OpenSfM

[3] https://github.com/cdcseacave/openMVS

(a) Placement of cameras. (b) Corresponding images of viewpoints.

Figure 1: The eight predetermined camera viewpoints at the construction site. Cameras are positioned to continuously monitor the site, capturing images day and night at varying frequencies—every 5 minutes during active construction hours.

3 DATASET

We deployed eight high-resolution (4K) and wide-angle view cameras at fixed positions across the construction site to collect a dataset. The corresponding viewpoints are illustrated in Figure 1. The cameras were mounted on cranes or poles, and their locations were chosen based on a comprehensive analysis of the site's layout, ensuring that each camera provided a unique viewpoint, thereby maximizing the coverage and minimizing the redundancy in the captured images.

To capture varying stages and activities of construction throughout the construction's entirety, the cameras were programmed to automatically capture images at different intervals. Between 6 a.m. and 7 p.m., images were taken every 5 minutes to closely monitor the most active period of construction activities. Conversely, during the less active hours, spanning from 7 p.m. to 6 a.m., the cameras captured images at 30-minute intervals.

4 METHOD

A pipeline is proposed for comparing the as-built building with the as-planned BIM model using the collected images, as illustrated in Figure 2. We first generate a point cloud representative of the as-built structure using the classical image-based 3D reconstruction pipeline that includes structure-from-motion (Section 4.1) and multi-view stereo (Section 4.2).

Upon the successful generation of the point cloud, a point cloud registration approach is subsequently employed to align the derived point cloud with the as-planned BIM model (Section 4.3).

4.1 Structure-from-Motion

The structure-from-motion (SfM) algorithm serves as a foundational mechanism to convert input images into outputs of camera parameters and a set of 3D points, referred to as a sparse model. Incremental SfM, recognized for its widespread application, implements this through a pipeline (Furukawa et al., 2015; Schönberger and Frahm, 2016), involving 1) feature detection and matching enhanced with geometric verification, 2) initialization of the foundation for the reconstruction stage via careful selection of two-view reconstruction, and 3) the registration of new images through triangulation of scene points, outlier filtration, and refinement of the reconstruction using bundle adjustment (BA).

4.1.1 Feature Extraction and Feature Matching

In the feature detection and matching stage of the SfM pipeline, the objective is to identify distinctive points in the images and establish accurate correspondences between them. Accurate feature extraction and matching play a pivotal role in achieving successful 3D reconstruction and camera pose estimation.

Traditional methods such as SIFT (Lowe, 2004) and SURF (Bay et al., 2006), based on handcrafted features, face challenges with viewpoint changes and repetitive patterns. Recent advancements in deep learning-based methods (LeCun et al., 2015; Ma et al., 2021) have shown superior performance in image matching. In our study, we utilize SuperPoint (DeTone et al., 2018) for efficient interest point detection and description, and SuperGlue (Sarlin et al., 2020) for robust feature matching.

4.1.2 Initialization

The initial selection of an appropriate image pair is crucial in the SfM process. Inadequate initialization can lead to reconstruction failures, and the subsequent robustness, accuracy, and performance of the incremental reconstruction heavily depend on this initial step. To have a more robust and accurate reconstruction, the initial image I_0 is selected in the image graph with the most overlapping cameras. A sequence of

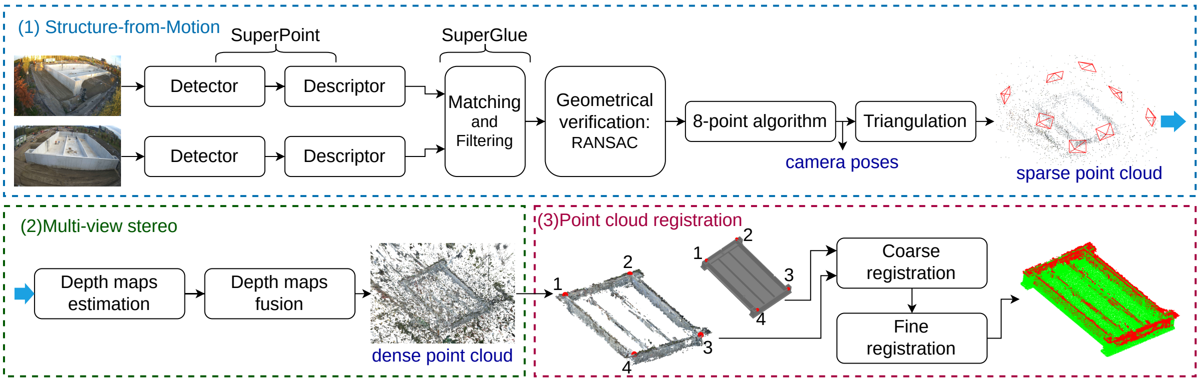

Figure 2: Proposed pipeline for comparing the as-built building with the as-planned BIM model. The pipeline includes, 1) estimating camera poses using structure-from-motion, 2) generating a dense point cloud using multi-view stereo, and 3) aligning the created point cloud with BIM model using point cloud registration. Note that noise points are manually removed from the dense point cloud before performing point cloud registration, and the BIM model is converted into a point cloud from a mesh.

images is then determined by prioritizing pairs with the highest match count, starting with (I_0, I_1). Iteratively, for a given image I_k in the sequence, the next image I_{k+1} is selected based on its maximum match count with I_k from the set of unsequenced images. Image I_{k+1} is then appended to the sequence and removed from the set of unsequenced images. This procedure continues until all images are sequenced or no matches can be found for the most recent image in the sequence.

With the initial image pair (I_0, I_1), the eight-point algorithm is used to calculate the initial model (Hartley and Zisserman, 2003).

In the use case of two camera views, the epipolar constraint between the cameras is given by:

$$\mathbf{p_2}^T \mathbf{K}^{-\mathbf{T}} \mathbf{E} \mathbf{K}^{-\mathbf{1}} \mathbf{p_1} = 0. \tag{1}$$

Here, $\mathbf{p_1}$ and $\mathbf{p_2}$ represent the corresponding 2D points in the first and second camera views for a 3d point $\mathbf{P}$, which are the matches keypoints obtained in the step of feature extraction and matching. $\mathbf{K}$ is the intrinsic parameters of the cameras. $\mathbf{E}$ is the essential matrix represented as $E = [t]_\times \mathbf{R}$, where $\mathbf{t}$ and $\mathbf{R}$ correspond to the translation vector and rotation matrix, respectively, with $[t]_\times$ being the skew-symmetric matrix associated with $\mathbf{t}$ (Hartley and Zisserman, 2003). To estimate the translation vector $\mathbf{t}$ and rotation matrix $\mathbf{R}$, the eight-point algorithm (Hartley, 1997; Longuet-Higgins, 1981) is used to calculate $\mathbf{E}$, followed by deriving the $\mathbf{t}$ and $\mathbf{R}$ using singular value decomposition (SVD) (Hartley and Zisserman, 2003). Since there are typically more than eight pairs of keypoints, and some matches may be incorrect, we utilize RANSAC (Fischler and Bolles, 1981) to filter out unreliable matches before estimating $\mathbf{E}$.

4.1.3 Triangulation

After obtaining camera poses for two viewpoints, we calculate the corresponding 3D points of matches between the two images using the Direct Linear Transform (DLT) method. This method leverages the projection matrices of the cameras and the corresponding points in the images (Hartley and Zisserman, 2003).

4.1.4 Register Next Images

Starting with the initial 3D model, each subsequent image from the image sequence, created during the initialization phase, is systematically aligned to the model. This registration is achieved by solving the Perspective-n-Point (PnP) problem (Furukawa et al., 2015) that estimates the camera pose from a set of 2D image feature correspondences and their corresponding 3D points. In our study, we adopted the RANSAC-based PnP method (Furukawa et al., 2015; Hartley and Zisserman, 2003). Subsequently, the estimated camera pose is used to calculate the 3D points of matches of the subsequent image, followed by adding the 3D points to the 3D model. To enhance the accuracy of the alignment, bundle adjustment is employed. This iterative alignment process continues until all images in the sequence have been registered.

4.1.5 Bundle Adjustment

Bundle adjustment (BA) aims to refine camera poses, intrinsic parameters, and 3D scene structure by iteratively minimizing the reprojection error. In incremental SfM, BA is processed after registering each image (Hartley and Zisserman, 2003).

Reprojection error quantifies the disparity between the observed 2D image points $\mathbf{u}_i$ and their corresponding projected 3D points $\mathbf{X}_i$ in the camera coordinate system. Given a set of N 2D image points $\mathbf{u}_i$ and their corresponding 3D points $\mathbf{X}_i$, and considering the camera projection matrix $\mathbf{P}$, the reprojection error E is defined as:

$$E = \sum_{i=1}^{N} \|\mathbf{u}_i - \mathbf{P}\mathbf{X}_i\|^2. \tag{2}$$

The goal of BA is to solve for the optimal camera parameters $\mathbf{P}$ and 3D scene points $\mathbf{X}$ that minimize the reprojection error across all observed image points. This iterative optimization process ensures that the reconstructed 3D scene aligns more accurately with the observed 2D image data, resulting in improved reconstruction fidelity.

4.2 Multi-View Stereo

Multi-view stereo (MVS) aims to create a dense point cloud of a scene using multiple images with known camera poses. Depth map estimation and fusion are the main steps in classical MVS (Furukawa et al., 2015). In our study, we obtain image correspondences and camera parameters during the SfM step, followed by image rectification. Since our goal is to generate a dense point cloud, we primarily focus on depth map estimation and fusion in this section.

Depth map estimation aims to assign a depth value to each pixel in an image, representing the distance from the camera to the corresponding point in the scene (Hartley and Zisserman, 2003; Pollefeys et al., 2008). The challenge in this step is to ascertain the depth that maximizes both photo-consistency and geometry-consistency across multiple images for each pixel. Photo-consistency ensures that the appearance of a point is consistent across different views, while geometry-consistency ensures that the reconstructed 3D point is geometrically plausible and consistent with neighboring points in terms of depth and surface normals. For robust and accurate depth map estimation, we adopt the PatchMatch stereo (Bleyer et al., 2011; Barnes et al., 2009) algorithm, which optimizes correspondences between patches (small regions in stereo images) instead of individual pixels.

Depth map fusion aims to create a 3D point cloud of a scene by integrating depth maps. The typical procedure begins by refining depth values using probability masks, followed by visibility filtering across multiple viewpoints to improve accuracy. Afterward, the refined depth maps are back-projected into 3D space to generate point clouds. These constructed point clouds are then combined, resulting in a detailed and accurate 3D representation of the scene (Furukawa et al., 2015).

4.3 Alignment of Point Cloud and BIM Model

The generated point cloud is aligned to the BIM model using a point cloud registration method. Point cloud registration aims to find the transformation (rotation, translation, and possibly scaling) that minimizes the distance between corresponding points in two point clouds, which typically unfolds in two main stages: coarse registration and fine registration (Besl and McKay, 1992).

Coarse registration, the initial phase in point cloud alignment, seeks an approximate transformation between point clouds, typically using methods like feature matching or geometric primitives (Rusinkiewicz and Levoy, 2001; Chetverikov et al., 2002). Due to incomplete point clouds from ongoing construction in our study, we manually select corresponding points and compute the transformation matrix using Singular Value Decomposition (SVD) of the cross-covariance matrix between the point sets (Arun et al., 1987; Besl and McKay, 1992; Eggert et al., 1997).

Consider points $\mathbf{A} = (\mathbf{a}_1, \mathbf{a}_2, \ldots, \mathbf{a}_n)$ and $\mathbf{B} = (\mathbf{b}_1, \mathbf{b}_2, \ldots, \mathbf{b}_n)$ to be the corresponding manually picked points for the BIM model and the generated point cloud, respectively. To align the generated point cloud to the BIM model, we align the points $\mathbf{B}$ to $\mathbf{A}$. We first compute the centroids $\mathbf{c_A}$ and $\mathbf{c_B}$ as follows:

$$\mathbf{c_A} = \frac{1}{N} \sum_{i=1}^{N} \mathbf{a}_i, \tag{3}$$

$$\mathbf{c_B} = \frac{1}{N} \sum_{i=1}^{N} \mathbf{b}_i. \tag{4}$$

Next, we translate both points such that their centroids are at the origin, resulting in the centered points $\bar{\mathbf{A}}$ and $\bar{\mathbf{B}}$:

$$\bar{\mathbf{A}} = \mathbf{A} - \mathbf{1}^\top \mathbf{c_A}, \tag{5}$$

$$\bar{\mathbf{B}} = \mathbf{B} - \mathbf{1}^\top \mathbf{c_B}, \tag{6}$$

where $\mathbf{1} = (1_1, \ldots, 1_N)$.

The cross-covariance matrix $\mathbf{H}$ between the centered point sets is computed as:

$$\mathbf{H} = \sum_{i=1}^{N} \bar{\mathbf{B}}_\mathbf{i} \otimes \bar{\mathbf{A}}_\mathbf{i}, \tag{7}$$

where $\otimes$ denotes the outer product of two vectors. Using SVD on $\mathbf{H}$, we decompose it as:

$$\mathbf{H} = \mathbf{U}\mathbf{\Sigma}\mathbf{V}^T, \tag{8}$$

from which the rotation matrix $\mathbf{R}$ is derived as:

$$\mathbf{R} = \mathbf{V}^T \mathbf{U}^T. \tag{9}$$

The scaling factor s is then computed based on the ratio of the norms of the centered points:

$$s = \frac{\sum_{i=1}^{N} ||\bar{\mathbf{A}}_{\mathbf{i}}||_2}{\sum_{i=1}^{N} ||\mathbf{R}\bar{\mathbf{B}}_{\mathbf{i}}||_2}. \tag{10}$$

With the rotation matrix $\mathbf{A}$ and scaling factor s, the translation vector $\mathbf{t}$ is computed as:

$$\mathbf{t} = C_{\mathbf{A}} - s\mathbf{R}C_{\mathbf{B}}. \tag{11}$$

Finally, the transformation matrix $\mathbf{T}_c$ is constructed in homogeneous coordinates as:

$$\mathbf{T}_c = \begin{bmatrix} s\mathbf{R} & \mathbf{t} \\ \mathbf{0} & 1 \end{bmatrix}. \tag{12}$$

After coarse registration, fine registration refines the alignment to achieve high-precision alignment between the aligned point cloud and the BIM model. The Iterative Closest Point (ICP) algorithm is a widely-used method for fine registration (Besl and McKay, 1992). In our case, we employ the point-to-point ICP algorithm that iteratively minimizes the distance between corresponding points until predefined convergence criteria are met, typically based on a maximum number of iterations.

5 REPROJECTION ERROR OF SfM IN METRIC UNITS

The purpose of analyzing the reprojection error in metric units is to quantify the error using the metric units of the BIM model so that it can become meaningful for construction sector specialists.

To achieve this, we initially use the point cloud as a reference and align the BIM model with the point cloud using a coarse point cloud registration method, as discussed in Section 4.3. This alignment yields two point sets: $\mathbf{A}$ $(\mathbf{a}_1, \mathbf{a}_2, \ldots, \mathbf{a}_i)$ for the point cloud and $\mathbf{B}$ $(\mathbf{b}_1, \mathbf{b}_2, \ldots, \mathbf{b}_i)$ for the aligned BIM model.

For a single viewpoint, we back-project the point sets $\mathbf{A}$ and $\mathbf{B}$ onto the 2D image plane, yielding point sets $\mathbf{A}' = (\mathbf{a}'_1, \mathbf{a}'_2, \ldots, \mathbf{a}'_i)$ and $\mathbf{B}' = (\mathbf{b}'_1, \mathbf{b}'_2, \ldots, \mathbf{b}'_i)$, respectively. The reprojection error of SfM, expressed in metric units and corresponding to a single point in the BIM model, is calculated as:

$$E_{SfM} = \frac{D(a_i, b_i)\,\lambda}{D(a'_i, b'_i)}\,E_{re}, \tag{13}$$

where $D(\cdot)$ denotes the Euclidean distance, λ is the unit distance in metric units derived from the BIM model coordinate system, and E_{re} is the reprojection error of SfM in pixel.

6 RESULT

A 3D point cloud of the construction site was successfully generated using images from only eight distinct viewpoints. The 3D point cloud of the construction site is generated using images captured at different times, accounting for the varying illumination conditions throughout the day.

Figure 3a presents a dense point cloud generated using images from the eight viewpoints taken during daylight, with each viewpoint represented by a single image. A section of a wall failed to be reconstructed due to the absence of matches in the reflective area, as highlighted in Figure 3d. In contrast, Figure 3b displays a point cloud generated from nighttime images, where a wall section, annotated by a green dotted line, remains unreconstructed. Given that the construction site is treated as a static scene, image features are influenced by the texture of the building, which fluctuates with changing outdoor illumination. By merging images taken at different times, the texture diversity is enhanced, leading to increased image features and matches. This approach facilitates a more complete point cloud representation of the building. For example, the point cloud in Figure 3c was reconstructed using images that were used to create the two previously mentioned point clouds, including four walls. We applied this method to create a dense model for the complete building, resulting in a SfM reprojection error (E_{re}) of 0.72 pixels.

In the coarse registration step, the four corners of the building were selected as correspondences, as shown in Figure 2. Using the homography derived from the alignment, we computed the reprojection error of SfM in metric units. The mean of SfM reprojection error in metric units across all viewpoints is 4.17 cm, and the ranges of each viewpoint are presented in Table 1. The table clearly shows that reprojection errors differ among viewpoints, with a larger spread in maximum errors (7.86 cm) compared to minimum errors (1.96 cm). The error could be caused by imprecise camera pose estimations. Moreover, the generated dense point is incomplete and has holes because of sparse views, which may cause inaccuracies in manually selected points during the point cloud registration step, resulting in reprojection errors. However, excluding the maximum error of the sixth viewpoint, all SfM projection errors are under 10 cm, which is acceptable for a building measuring 30.15 meters in width and 47.15 meters in length from a perspective of construction sector.

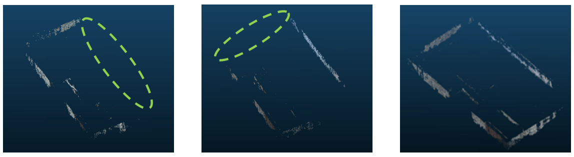

(a) (b) (c)

(d)

(e)

Figure 3: Dense model generated using (a) images captured during the daytime, (b) images captured at nighttime, and (c) images captured during both daytime and nighttime. Matches in image pairs captured (d) during the daytime and (e) at nighttime.

Table 1: Statistics of the SfM reprojection error in centimeters (cm) of each viewpoint.

Viewpoint	1	2	3	4	5	6	7	8
min	1.85	2.07	1.02	1.91	2.98	2.04	1.31	1.4
mean	2.89	4.66	3.6	3.53	3.45	6.3	4.02	3.89
median	2.89	3.73	3.8	3.47	3.45	5.69	3.22	3.75
max	3.93	9.12	5.77	5.28	3.93	11.79	8.34	6.66

7 APPLICATION

Using the homography derived from aligning the point cloud with the BIM model, we tracked activities on the construction site by locating workers within the BIM coordinate system. For a given timestamp, we initiated by generating bounding boxes for workers on images captured from various viewpoints (as shown in Figure 4a). Subsequently, masks were created for each of these images. Leveraging the shape-from-silhouette method (Laurentini, 1994), we created voxel volumes representing the workers. These voxel volumes were transformed using the obtained homography and were then visualized in conjunction with the BIM model, as depicted in Figure 4b.

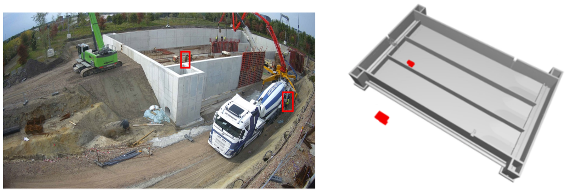

(a) (b)

Figure 4: Tracking activities using the homography obtained in the alignment. (a) Bounding boxes of workers in an image. (b) Visualizing voxel volumes of workers within the BIM coordinate system.

8 CONCLUSION

In this study, we collected images from eight fixed camera viewpoints at an actual construction site. To spatially position construction activities within the BIM coordinate system, we employed classical multi-view stereo techniques to generate a 3D point cloud of the as-built building, followed by aligning the point cloud with the as-planned BIM model using a cloud registration approach. We proposed an algorithm to convert SfM reprojection error into a value with metric units, resulting in a mean SfM reprojection error of 4.17 cm. This result is considered acceptable within the construction sector. We further visualized the construction activities by creating voxel volumes and integrating them with the BIM model using the result of the alignment.

REFERENCES

Ahmed, S. (2019). A Review on Using Opportunities of Augmented Reality and Virtual Reality in Construction Project Management. *Organization, Technology and Management in Construction: an International Journal*, 11:1839 – 1852.

Arun, K. S., Huang, T. H., and Blostein, S. D. (1987). Least-squares fitting of two 3-D point sets. *IEEE Transactions on Pattern Analysis and Machine Intelligence*, PAMI-9(5):698–700.

Azhar, S. (2011). Building information modeling (BIM): Trends, benefits, risks, and challenges for the AEC industry. *Leadership and management in engineering*, 11(3):241–252.

Barnes, C., Shechtman, E., Finkelstein, A., and Goldman, D. B. (2009). PatchMatch: A randomized correspondence algorithm for structural image editing. *ACM Trans. Graph.*, 28(3):24.

Bay, H., Tuytelaars, T., and Van Gool, L. (2006). SURF: Speeded Up Robust Features. In *European Conference on Computer Vision*, pages 404–417. Springer.

Besl, P. J. and McKay, N. D. (1992). A Method for Registration of 3-D Shapes. *IEEE Transactions on Pattern Analysis and Machine Intelligence*, 14(2):239–256.

Bleyer, M., Rhemann, C., and Rother, C. (2011). Patchmatch stereo-stereo matching with slanted support windows. In *BMVC*, volume 11, pages 1–11.

Chetverikov, D., Svirko, D., Stepanov, D., and Krsek, P. (2002). Robust Euclidean alignment of 3-D point sets: the trimmed iterative closest point algorithm. *Image and Vision Computing*, 20(12):1071–1077.

DeTone, D., Malisiewicz, T., and Rabinovich, A. (2018). SuperPoint: Self-Supervised Interest Point Detection and Description. In *Conference on Computer Vision and Pattern Recognition*, pages 224–233.

Eggert, D. W., Lorusso, A., and Fisher, R. B. (1997). Estimating 3-D Rigid Body Transformations: A Comparison of Four Major Algorithms. In *Computer Vision and Pattern Recognition, 1997. Proceedings., 1997 IEEE Computer Society Conference on*, pages 699–704. IEEE.

Fischler, M. A. and Bolles, R. C. (1981). Random sample consensus: a paradigm for model fitting with applications to image analysis and automated cartography. *Communications of the ACM*, 24(6):381–395.

Furukawa, Y., Hernández, C., et al. (2015). Multi-view stereo: A tutorial. *Foundations and Trends® in Computer Graphics and Vision*, 9(1-2):1–148.

Golparvar-Fard, M., Peña-Mora, F., and Savarese, S. (2009). D4AR–a 4-dimensional augmented reality model for automating construction progress monitoring data collection, processing and communication. *Journal of information technology in construction*, 14(13):129–153.

Hartley, R. and Zisserman, A. (2003). *Multiple view geometry in computer vision*. Cambridge university press.

Hartley, R. I. (1997). In defense of the eight-point algorithm. *IEEE Transactions on pattern analysis and machine intelligence*, 19(6):580–593.

Karsch, K., Golparvar-Fard, M., and Forsyth, D. (2014). ConstructAide: analyzing and visualizing construction sites through photographs and building models. *ACM Transactions on Graphics (TOG)*, 33(6):1–11.

Khalid Masood, M., Aikala, A., Seppänen, O., Singh, V., et al. (2020). Multi-Building Extraction and Alignment for As-Built Point Clouds: A Case Study With Crane Cameras.

Kim, C., Ju, Y., Kim, H., and Kim, J. (2009). Resource management in civil construction using RFID technologies. In *Proceedings of the 26th International Symposium on Automation and Robotics in Construction (ISARC 2009), Austin, TX, USA*, volume 2427, page 105108. Citeseer.

Kim, D., Liu, M., Lee, S., and Kamat, V. (2019). Remote proximity monitoring between mobile construction resources using camera-mounted UAVs. *Automation in Construction*.

Laurentini, A. (1994). The visual hull concept for silhouette-based image understanding. *IEEE Transactions on pattern analysis and machine intelligence*, 16(2):150–162.

LeCun, Y., Bengio, Y., and Hinton, G. (2015). Deep learning. *Nature*, 521(7553):436–444.

Longuet-Higgins, H. C. (1981). A computer algorithm for reconstructing a scene from two projections. *Nature*, 293(5828):133–135.

Lowe, D. G. (2004). Distinctive image features from scale-invariant keypoints. *International journal of computer vision*, 60:91–110.

Ma, J., Jiang, X., Fan, A., Jiang, J., and Yan, J. (2021). Image matching from handcrafted to deep features: A survey. *International Journal of Computer Vision*, 129:23–79.

Mahami, H., Nasirzadeh, F., Hosseininaveh Ahmadabadian, A., and Nahavandi, S. (2019). Automated progress controlling and monitoring using daily site images and building information modelling. *Buildings*, 9(3):70.

Oh, S.-W., Chang, H.-J., Kim, Y.-S., Lee, J., and Kim, H.-s. (2004). An Application of PDA and Barcode Technology for the Improvement of Information Management in Construction Projects.

Pollefeys, M., Nistér, D., Frahm, J.-M., Akbarzadeh, A., Mordohai, P., Clipp, B., Engels, C., Gallup, D., Kim, S.-J., Merrell, P., et al. (2008). Detailed real-time urban 3d reconstruction from video. *International Journal of Computer Vision*, 78:143–167.

Rusinkiewicz, S. and Levoy, M. (2001). Efficient variants of the ICP algorithm. In *Proceedings Third International Conference on 3-D Digital Imaging and Modeling*, pages 145–152. IEEE.

Sami Ur Rehman, M., Shafiq, M. T., and Ullah, F. (2022). Automated Computer Vision-Based Construction Progress Monitoring: A Systematic Review. *Buildings*, 12(7):1037.

Sarlin, P.-E., DeTone, D., Malisiewicz, T., and Rabinovich, A. (2020). SuperGlue: Learning Feature Matching with Graph Neural Networks. In *European Conference on Computer Vision*, pages 815–832.

Schönberger, J. L. and Frahm, J.-M. (2016). Structure-from-Motion Revisited. In *Conference on Computer Vision and Pattern Recognition (CVPR)*.

Sepasgozar, S., Lim, S., Shirowzhan, S., and Kim, Y. M. (2014). Implementation of As-Built Information Modelling Using Mobile and Terrestrial Lidar Systems. pages 876–883.

Tuttas, S., Braun, A., Borrmann, A., and Stilla, U. (2017). Acquisition and consecutive registration of photogrammetric point clouds for construction progress monitoring using a 4D BIM. *PFG–journal of photogrammetry, remote sensing and geoinformation science*, 85(1):3–15.

Xue, J., Hou, X., and Zeng, Y. (2021). Review of image-based 3D reconstruction of building for automated construction progress monitoring. *Applied Sciences*, 11(17):7840.

Zhang, J., Zhang, J., Mao, S., Ji, M., Wang, G., Chen, Z., Zhang, T., Yuan, X., Dai, Q., and Fang, L. (2021). GigaMVS: a benchmark for ultra-large-scale gigapixel-level 3D reconstruction. *IEEE Transactions on Pattern Analysis and Machine Intelligence*, 44(11):7534–7550.